Bulgarian Chemical Communications, Volume 50, Special issue L (pp. 341 – 347) 2018

Synthesis of porous Al_2O_3–SiO_2 nanocomposite xerogel through a sol-gel method and its application in adsorption of heavy metals

Sh. Bizhanzadeh[1], M. Daghighi[1]*, L. Torkian[2]

[1]*Department of Chemistry, College of Basic Sciences, Central Tehran Branch, Islamic Azad University, Tehran, Iran*

2Research Center of Modeling and Optimization, South Tehran Branch, Islamic Azad University, Tehran, Iran

Submitted March 24, 2016; Accepted August 8, 2016

Various methods have been presented by different researches for the synthesis of Al_2O_3–SiO_2 nanocomposite xerogel based on its different applications in industries. In this research, a simple, economic and environmental friendly method was presented for the preparation of Al_2O_3-SiO_2 nanocomposite xerogel using sol-gel method. The structure of prepared nanocomposites is characterized by FTIR, BET, SEM, XRD and EDX methods. To consider the effect of product calcinations on porosity, specific surface area, diameter, volume and distribution of pore size calcinated at temperatures of 600, 800 and 1200 °C, nitrogen adsorption/desorption device was used. Results from the study of isothermal charts confirm the mesoporous structure of prepared nanocomposites and their highest specific surface area among known Alumina –Silica zerogel synthesized nanocomposites. The nanocomposite can be utilized as an adsorbent due to its homogeneity and porosity. Therefore, In order to study the absorption of heavy metals, lead and nickel adsorption by nanocomposite calcinated at temperatures of 600, 800 and 1200 °C was studied in this research and atomic absorption spectrometry (AAS) was employed for the calculation of Pb (II) and Ni(II) concentrations. Results from AAS indicate that all three samples have good potentials in adsorption of mentioned cations while lead adsorption is more efficient than nickel.

Keywords: Al_2O_3-SiO_2 nanocomposite xerogel ؛ porosity ؛ mesoporous ؛ specific surface area؛ adsorbent

INTRODUCTION

Active alumina is a porous aluminum oxide whose specific surface area is 200 m^2/g or above, and the volume of its pores is also large [1]. Active alumina is widely utilized as a catalyst and adsorbent. Some of its uses include supporting defluorization of drinking water [1-3] and heavy metals removal from water [4-5], production of special electric compounds [6,7], as adsorbent in liquid and gas treatment processes [8], as solid electrolyte in battery for electric vehicles and energy storage systems [9], as catalyzer in heterogeneous decomposition [10,11], and ion exchange processes [12]. In addition, silica particles also have good size and morphology and have extensive usage in various areas including adsorption, separation techniques, chromatography, and catalysts [13-17].

Addition of alumina to silica not only increases the chemical stability of Al_2O_3-SiO_2 nanocomposite, but it also causes increased specific surface area and development of unique properties and characteristics [18]. Different methods can be employed to produce these compounds with a high purity [19]. Spray drying, hydrothermal technique, hydrolysis, and etc. are among these methods. Meanwhile, sol gel method possesses more advantages than other techniques including high purity, very good chemical homogeneity, and low processes temperature [19-21]. In 1956, Roy [22] first prepared Al_2O_3 and SiO_2 mixture out of tetra ethyl orthosilicate (TEOS) and aluminum nitrate Nano hydrate (ANN). Thereafter, some scientists used various organic and inorganic compounds to synthesize this composite employing sol-gel method [23-37]. According to published researches, synthesized nanoparticles belong to porous compounds. According to IUPAC classification, the structure of a porous medium is classified into three groups based on the mean dimension of the pores: micropores with a diameter of less than 2 nm, mesopores with a diameter of 2-50 nm, and macropores with pores larger than 50 nm. The term "nanoporous materials" has been used for compounds with a pore diameter below 100 nm. Porous solids with a high surface area are utilized as adsorbent, catalyst, and catalytic supports [37-42].

One of the most important uses of nanoporous materials in recent years has been the adsorption of a variety of contaminants. Adsorption is considered a stable separation process and an effective solution to decontaminating water. The adsorption process have some advantages in comparison to other methods, as it treats water and prepares it for reuse with a low cost, high flexibility, simple design and development, and high sensitivity to toxic materials. Moreover, it does not develop hazardous compounds [39-41]. Thus, this process, employing porous nanoadsorbents is very efficient and of interest to scientists.

This study aims to prepare the composite nanopowder of Al_2O_3-SiO_2 xerogel with a simple, economical, and environmentally friendly method. In this method, first silica sol and alumina sol were mixed with each other, followed by gelling, ageing, drying, and calcination across various temperatures. Subsequently, the extent of porosity of the calcinated products was examined at temperatures of 600, 800, and 1200 °C.

The Al_2O_3-SiO_2 sol was prepared utilizing an inexpensive inorganic salt ($AlCl_3.6H_2O$) and tetra othoxy orthosilicate (TEOS) as the precursor instead of alumina and silica nano powder. Ethanol was employed as the solvent and propylene oxide (PO) was used as the gel accelerator.

EXPERIMENTAL

Al_2O_3-SiO_2 nanocomposite xerogel powder with values of 80 and 20 wt% alumina to silica were prepared according to the following three steps.

In the first stage, appropriate amount of 25. 5 ml of H_2O and 28.5ml of C_2H_5OH were mixed, and then 8.0g of $AlCl_3$.$6H_2O$ was dissolved in the mixture, while stirring was done for about 30 min for complete hydrolysis.

In the second stage, 2.154 ml of TEOS was added to a mixture comprising 0.7 ml H_2O and8.9 ml C_2H_5OH. The mixed solution was continuously stirred for about 90 min at 50°C and then cooled to room temperature.

Finally, in the third phase, the silica sol and alumina sol were mixed together at room temperature, and then a desired amount of 18.8 ml propylene oxide (PO) was poured into the clear solution. The reaction mixture was further stirred for 10 min and the solution was gel at room temperature. The wet gel was aged at room temperature for 1 day and then dried at 60 °C for 12 h. Thereafter, the dried product was calcined at 600, 800 and 1200°C for 2 h to yield the calcined powder.

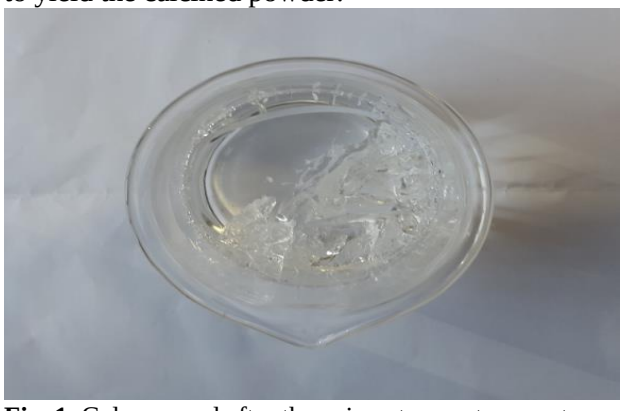

Fig. 1. Gel prepared after the aging at room temperature for 1 day

MATERIALS AND EQUIPMENT

TEOS and aluminum chloride ($AlCl_3.6H_2O$), Nickel II, nitrate (Ni $(NO_3)_2$. $6H_2O$), lead II nitrate (Pb $(NO_3)_2$.$6H_2O$), propylene oxide (PO), ethanol, and acetone were purchased from Merck. Co, Germany. In the synthesis stages, deionized distilled water was used. X-ray spectroscopy was carried out using X-ray diffraction device (Philips) equipped with copper lamp (Cu-Ka). Fourier transform Infrared spectroscopy (Japan−FT−IR−JASCO−410) was employed to detect the chemical structure of the samples. Characterization of the morphology of the products was performed using scanning electron microscopy (SEM) device. To identify the type and level of the elements of the resulting nanocomposite, X-ray diffraction energy analysis (XDE) was used. The specific area, volume of pores, and the mean diameter of pores were measured according to BET test.

DISCUSSION AND CONCLUSION

Studying FT-IR spectrum

Fig. 2 shows the FT-IR spectrum of Al_2O_3–SiO_2 xerogel nanocomposite. In its 25°C sample, two characteristic peaks were observed at 3477 and 1644 cm^{-1}, which are related to the stretching and bending vibrations of the adsorbed water, respectively.

Some peaks can be seen within the range of 1000 and 3500 cm^{-1}, which are related to the CO_2 and H_2O in the sample structure, respectively [43-45]. The peak at 2362 cm^{-1} is associated with the CO_2 in the air [46]. Adsorption at 2975, 2884, and 1455 cm^{-1} is associated with the bending vibrations of aliphatic carbons. The adsorption band at 1040 cm^{-1}, which can be seen with a suitable intensity, along with the bands at 572, 640, 447, and 835 cm^{-1} are related to pseudoboehmite Al-O vibrations [47].

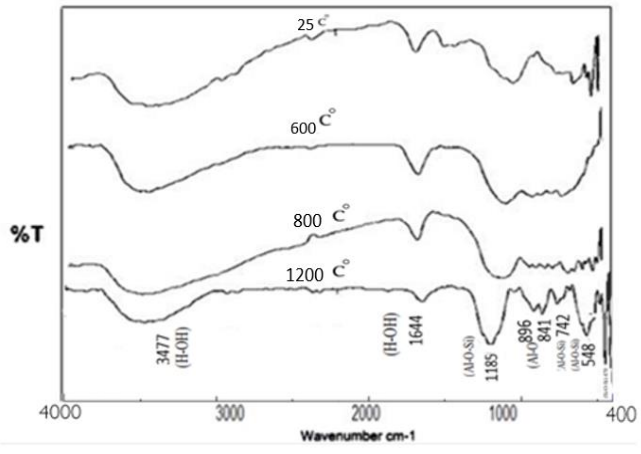

Fig. 2. FT-IR spectrum of Al_2O_3–SiO_2 xerogel nanocomposite across various temperatures

This band is no longer seen after reaching the temperature of 600°C. As the temperature reaches 800°C, a peak is observed at 841 cm^{-1} throughout heat operations, which is related to γ-Al_2O_3, which exists up to 1200°C. This peak is more conspicuous at 1200°C. According to the report of Li et al, alumina and silica form multiphase throughout heat operations. Therefore, the adsorptions observed at 1185, 742, and 548 cm^{-1} are associated with the development of Al-O-Si bonds [48].

Examination of X-ray diffraction pattern

The X-ray diffraction pattern of Al_2O_3–SiO_2 xerogel nanocomposite over heat operations is shown in Fig.3 across various temperatures. The wide peaks indicated for the 25°C sample at the regions of 27, 39, 65, 50, and 72°-2θ are related to pseudoboehmite [47,49]. At temperatures of 600 and 800°C, the nano composite is amorphous. This amorphous shape indicates lack of emergence of any crystal phase in the X-ray diffraction pattern related to the sample. Only amorphous peak emerged at the angle of 25°. It can be concluded that silica prevents crystallization of aluminum oxide due to its amorphous structure [50]. Therefore, aluminum oxide emerges with wide peaks in the diffraction pattern [51]. The EDX spectrum, which is shown in Fig. 4, confirms the presence of Al and Si elements. With the continuation of heat operations up to 1200°C, the X-ray diffraction pattern indicates that at this temperature, crystallization has occurred, where multiphases, γ-Al_2O_3, and silica are observed. Thus phase transition has occurred from the initial boehmite phase two γ-Al_2O_3 as well as the initial structure of SiO_2 which has been amorphous to silica, and multiphase of Al_2O_3-SiO_2 has also been developed.

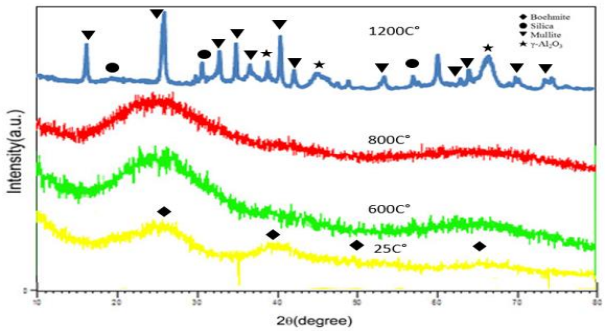

Fig. 3. The XRD pattern of Al_2O_3–SiO_2 xerogel nanocomposite over the heat operations across various temperatures

The diffraction pattern indicated in Fig. 3 confirms the formation of Al_2O_3–SiO_2 xerogel nanocomposite according to the standard card number 01_079_1453. Using Debi-Scherer equation, calculation of the mean size of crystal was performed using X-ray at a temperature of 1200°C [52]. The crystal size of the synthesized nanocomposite is about 65 nm.

X-ray diffraction energy spectroscopy (EDX)

The distribution percentage of atoms in the structure of the nanocomposite, which has been determined using EDX detector, is presented in Table 1.

Table 1. The distribution percentage of the elements in the nanocomposite Al_2O_3–SiO_2

Sample	C	O	Al	Si
A%	5.84	49.85	34.67	9.64
W%	3.38	38.46	45.11	13.05

Fig. 4. Energy dispersive X-ray spectroscopy (EDX) in the nanocomposite Al_2O_3–SiO_2

In Table 1, the elements present in the structure of Al_2O_3–SiO_2 xerogel nanocomposite have been indicated in the form of a weight percentage and atomic percentage. The value of each of these compounds in terms of weight percentage and atomic percentage has relatively a good congruence with the value of the initial feed. This implies that the weight ratio of Al/Si was 3.45 in the initial mixture, which is almost equivalent to the ratio in the product (Al/Si=3.32).

Morphology of the nanocomposite using scanning electron microscopy (SEM)

To examine the morphology, size, geometric shape of the particles and the status of the porosity of the nanoparticles over heat operations across the temperatures of 600, 800, and 1200°C, scanning electron microscopy was used (Fig. 5). From 600°C onwards, the boundary of the grains is detectable and with increase in the calcination temperature, the degree of agglomeration was increased and the size of the particles grew from about 20 nm, at 800°C to about 65 nm at 1200°C. Overall, with increase in the calcination temperature, the size of the nanoparticles increases due to their agglomeration [53-56].

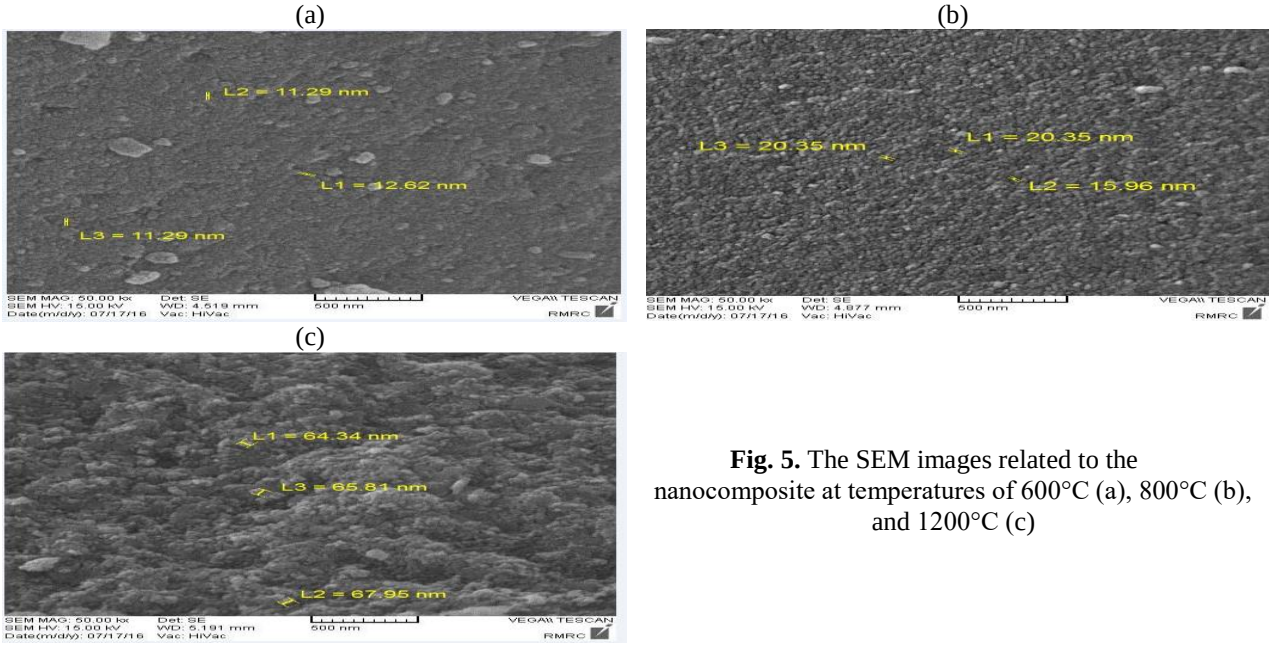

Fig. 5. The SEM images related to the nanocomposite at temperatures of 600°C (a), 800°C (b), and 1200°C (c)

Porosity study

Nitrogen adsorption and desorption device was utilized to examine the type of porosity, the specific surface area, diameter, and volume of the pores. Figs. 6, 7, 8, and 9 illustrate the nitrogen adsorption and desorption diagrams alongside the manner of size distribution of the Al_2O_3–SiO_2 xerogel nanocomposite over the heat operations across various temperatures. According to IUPAC classification, the isothermal diagrams are of 6 types, confirming the mesoporosity of the porous compound. Existence of a waste ring between the nitrogen adsorption and desorption branch on the surface is attributed to capillary condensation in the pores of the mesoporous compounds. Accordingly, cylindrical pores have been adsorbed because of gas liquidification. The delay developed during desorption is one of the characteristics of mesoporous compounds. Moreover, in these isothermal diagrams, the waste ring is of H_1 type. The special shape of each ring is due to its special pore structure, where H_1 ring resulting from the pores is isomorphic and has the same size distribution. The presence of this ring in the samples confirms thin and identical size distribution as well as mesoporosity of the synthesized nanocomposite over heat operations across various temperatures [57, 58].

Figs. 6, 7, and 8b depict the isothermal diagram of the nanocomposite at 25, 600, and 800°C. Based on these figures, the waste ring is seen between the relative pressures of 0.4 and 0.8. At 1200°C, the waste ring lies within the pressure range of 0.5-0.9

Table 2. The structure of the pores over the heat operations across various temperatures

Heat treatment, temperature (°C)	Specific surface area (m^2/g)	Average pore diameter (nm)	Pore volume (cm^3/g)
25	460.22	2.8133	0.3242
600	418.96	3.8699	0.4050
800	337.24	4.0506	0.34
1200	35.606	17.777	0.1582

The information adopted from BET is shown in Table 2. As can be seen in this table, with increase in temperature, the specific surface area has declined as a result of structural modification, damage to the network of the pores, and shrinkage of the structure [58]. In addition, it can be stated that the reduction in the specific surface area with increase in temperature is due to alumina and silica doping and formation of multiphase. Nevertheless, the specific surface area reported is larger than that of other

samples published in different researches. For instance, Poco et al have reported the specific surface area of their synthesized alumina as 376 m^2/g at 25°C [59]. Furthermore, Sedaghat et al reported the specific surface area of their synthesized Al_2O_3–SiO_2 to be 120 m^2/g at 900°C [60]. Haoa et al also reported 224 m^2/g as the specific surface area of Al_2O_3–SiO_2 composite at 600°C [61].

Figs. 6, 7, 8, and 9 indicate the specific surface area curve (BET) and the size distribution of the pores. The range of the size distribution of the pores in the Al_2O_3–SiO_2 xerogel nanocomposite is normal, identical, and uniform.

The high surface area of the nanocomposite resulting from this research confirms its mesoporosity. In addition, the equal and uniform size distribution of the particles which belongs to diagram VI and ease of H_1 waste type, according to IUPAC verifies the efficiency of the resulting nanocomposite as both an adsorbent and catalyst.

a b

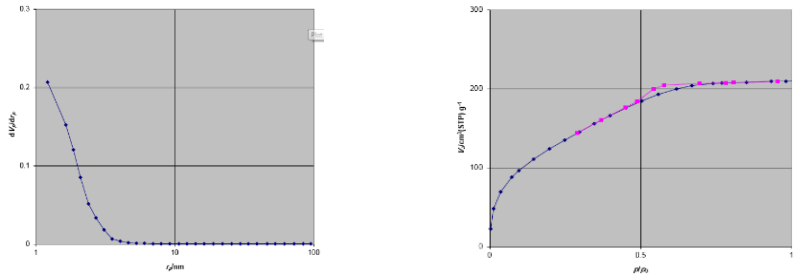

Fig. 6. (a) BJH pore size distribution and (b) N2 adsorption–desorption isotherm heat treated at25 °C.

a b

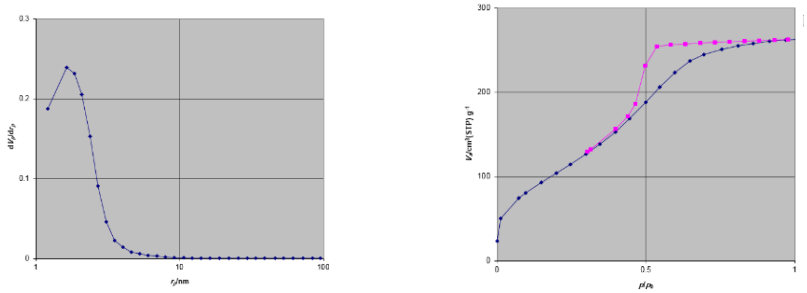

Fig. 7. (a) BJH pore size distribution and (b) N2 adsorption–desorption isotherm heat treated at600 °C.

a b

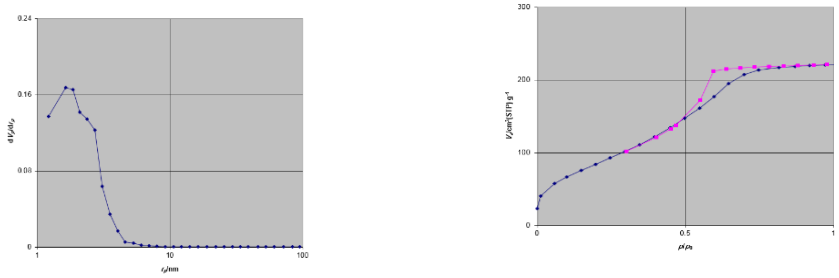

Fig. 8. (a) BJH pore size distribution and (b) N_2 adsorption–desorption isotherm heat treated at 800°C.

a b

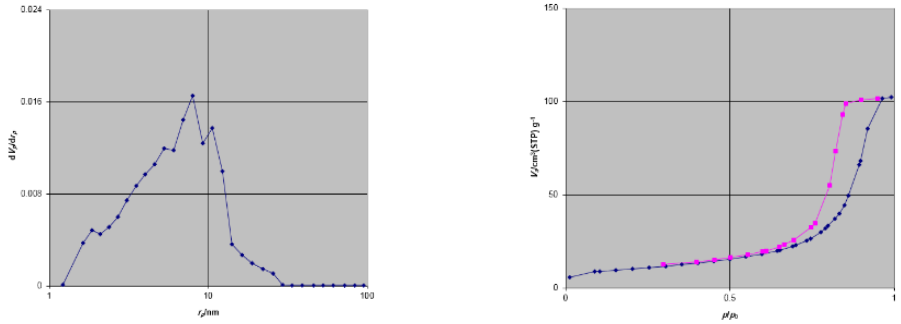

Fig. 9. (a) BJH pore size distribution and (b) N_2 adsorption–desorption isotherm heat treated at 1200°C.

Investigating the extent of adsorption of lead and nickel ions

Following preparation of the nanocomposites, their ability in adsorption of the ions of the heavy metals of lead and nickel was examined. For this purpose, solutions of the all ions of lead (II) and nickel (II) metals were prepared with a concentration of 20 mgL^{-1} as the initial solution. Then, 0.3 g of the Al_2O_3–SiO_2 nanocomposites, which had been calcinated across various temperatures and indicated as AS_{600}, AS_{800}, and AS_{1200} were added to the 20 mgL^{-1} solution as adsorbent, with the solution's pH being brought to 7. This solution was exposed to a shaker at 25°C at 500 rpm. After filtering, the samples were collected and the level of the metal was measured by atomic absorption device (AAS). The adsorption percentage of the metal and its value were calculated by the following relations:

The percentage of metal adsorption = ($C_\circ$- C_e) / $C_\circ$×100

Where, C_0 denotes the initial concentration of the metal in the solution (mgL^{-1}), C_e indicates the residual concentration of the metal in the solution (mgL^{-1}). Based on the results obtained, all three samples of the adsorbent have shown to be a good adsorbent for lead (II) and nickel (II), considering their good porosity, though they are better in removing lead than nickel (Table 3).

Table 3. The information related to the extent of ion adsorption by the AS_{600}, AS_{800}, and AS_{1200} adsorbents.

Adsorbent	Removal, %	
	Pb^{2+}	Ni^{2+}
AS_{600}	93.08	37.4
AS_{800}	95.38	55.45
AS_{1200}	95.38	43.6

CONCLUSION

In this research, Al_2O_3–SiO_2 xerogel nanocomposite was synthesized by sol gel method using inexpensive mineral salt and without using alumina and silica nanopowder within the shortest time interval. This method is simple, economical, and environmentally friendly. With increase in temperature up to 1200°C, crystallization occurred and multiphase, γ-Al_2O_3, and SiO_2 emerged. Accordingly, with heat operations up to 1200°C, there was improvement in nanocomposite network. Investigation of FT-IR spectrum confirms the formation of Al-Si-O bonds. The morphology of the nanocomposite by SEM indicates that the size of the particles increased from about 20 nm at 800°C to about 65 nm at 1200°C, which is in well congruence with the results obtained from Scherer equation and XRD spectrum.

The EDX spectrum confirms the presence of Al and Si elements. By examining the porosity of the samples across various temperatures using nitrogen adsorption and desorption diagrams, the mesoporosity of the porous compounds, the equal and uniform distribution of the pores, and their thin distribution were confirmed. The results obtained indicate the efficiency of the resulting nanocomposites as adsorbent and industrial catalysts. To confirm this important issue, the adsorption of lead (II) and nickel (II) ions was performed at 600, 800, and 1200°C with calcinated adsorbents. The results obtained indicated that the prepared nanocomposites are a good adsorbent for removing lead and nickel from water, but they are more effective in removing lead than nickel.

REFERENCES

1. A. Bansiwal, P. Pillewan, R.B. Biniwale, S. Sadhana Rayalu, *Microporous Mesoporous Mater*., **129**, 54 (2010).
2. J. Hao, M. Han, C. Wang, X. Meng, *Microporous Mesoporous Mater.*, **124**, 1 (2009).
3. G. Lee, C. Chen, C. Yang, W. Ahn, *Microporous Mesoporous Mater*., **127**, 52 (2010).
4. S. Naeem, U. Zafar, Pak. *J. Anal. Environ. Chem*., **10**, 83 (2009).
5. S. Jagtap, M.K.N. Yenkie, N. Labhsetwar, S. Rayalu, *Microporous Mesoporous Mater*., **142**, 434 (2011).
6. G. Jean, V. Sciamanna, M. Demuynck, F. Cambier, M. Gonon, *Ceram. Int*., **40**, 10197 (2014).
7. Z. Zheng, Y. Zhang, F. Yi, C. Chen, X. Song, *Ceram. Int*., **40**, 12709 (2014).
8. F. Glorias-Garcia, J. Arriaga-Merced, G. Roa-Morales, V. Varela-Guerrero, C.E. Barrera-Dı´az, B. Bilyeu, *J. Ind. Eng. Chem*., **20**, 2477 (2014).
9. W.J. Stępniowski, A. Nowak-Stępniowska, Z. Bojar, *Mater. Charact*., **78**, 79 (2013).
10. L. Miao, G. Ji, G. Gao, G. Li, S. Gan, *Powder Technol*., **207**, 343 (2011).
11. S.D. Ros, E. Barbosa-Coutinho, M. Schwaab, V. Calsavara, N.R.C. Fernandes-Machado, *Mater. Charact*., **80**, 50 (2013).
12. H. Yamada, A.J. Bhattacharyya, J. Maier, *Adv. Funct. Mater*., **16**, 525 (2006).
13. P. Wilhelm, C. Zetzsch, D. Stephan, *Progr. Colloid Polym. Sci*., **133**, 147 (2006).
14. T.M. Suzuki, M. Yamamoto, K. Fukumoto, Y. Akimoto, K. Yano, *J. Catal*., **251**, 249 (2007).

15. A. Ahmed, W. Abdelmagid, H. Ritchie, P. Myers, H.F. Zhang, *J. Chromatogr*., **A1270**, 194 (2012).
16. H.H. Wan, L. Liu, C.M. Li, X.Y. Xue, X.M. Liang, *J. Colloid. Interf. Sci*., **337**, 420 (2009).
17. Y.F. Zhu, J.L. Shi, W.H. Shen, H.R. Chen, X.P. Dong, M.L. Ruan, *Nanotechnology*, **16,** 2633 (2005).
18. J. Chandradass, D. Bae, *Materials and Manufacturing Processes*, **23**, 494 (2008).
19. C. W. Won, B. Siffert, *Colloid. Surface. A*, **131,** 161 (1998).
20. M. Schehl, L. A. Díaz, R. Torrecilla, *Acta Mater*., **50**, 1125 (2002).
21. S. Sakka, K. Kamiya, *J. Non-Cryst. Solids*, **42**, 403 (1980).
22. R. Roy, *J. Am. Ceram. Soc.*, **39,**145 (1956).
23. A. K. Chakraborty, *Thermochim. Acta*,**427** 109 (2005).
24. H. Schneider, S. Komarneni, Mullite, WILEY-VCH Verlag GmbH and Co. KGaA, Weinheim, 2005, pp. 263-272.
25. M. Yamane, S. Inoue, A. Yasumori, *J. Non-Cryst. Solids*, **63**, 13 (1984).
26. K. Okada, N. Otsuka, Characterization of Spinel Phase from SiO_2.Al_2O3 Xerogels and the Formation Process of Mullite, *J. Am. Ceram. So*c., **69**, 652 (1986).
27. A. K. Chakraborty, D. K. Ghosh, *J. Am. Ceram. Soc.*, **71,** 978 **(**1988).
28. Ch. Sh. Hsi, H. Y. Lu, F. S. Yen, *J. Am. Ceram. Soc*., **72**, 2208 (1989).
29. A. Yasumori, M. Anma, M. Yamane, *Phys. Chem. Glasses*, **30**, 193 (1989).
30. T. Heinrich, F. Raether, *J. Non-Cryst. Solids*, **147**/**148**, 152 (1992).
31. B. E. Yoldas, *J. Mater. Sci*., **27**, 66 (1992).
32. H. Schneider, B. Saruhan, D. Voll, L. Merwin, A. Sebald, *J. Eur. Ceram. Soc*., **11**, 87 (1993).
33. A. K. Chakraborty, *J. Mater. Sci*., **29**, 6131 (1994).
34. A. K. Chakraborty' *J. Mater. Sci.*, **29**, 1558 (1994).
35. Y. X. Huang, A. M. R. Senos, J. Rocha, J. L. Baptista, *J. Mater. Sci*., **32**, 105 (1997).
36. A. K. Chakraborty, S. Das, *Ceram. Int*., **29**, 27 (2003).
37. H. Kao, W. Wei, *J. Am. Ceram. Soc*., **83**, 362 (2000)
38. M. Zhu, *J. Chem*., **1**, 11 (2013).
39. G.A. Ozin, *Small*, **5**, 1240 (2009).
40. S. Sarkar, *J. Nanomaterials*,1, 5 (2014).
41. D.R. Mercier,; *Solid State Ionics*, **29,** 135 (2011).
42. Z.L.Teng, *Colloids and Surfaces A*, **384**, 200 (2011).
43. M.S. Ghodrati, M. Haghighi, J.S. Soltan−Mohammadzadeh, B. Pourabas, E. Pipelzadeh, *Reac. Kinet. Mech. Catal.*, **104**, 49 (2011).
44. Z. Abbasi, M. Haghighi, E. Fatehifar, S. Saedy, *Int. J. Chem. Reactor Eng.*, **9,** 1 **(**2011).
45. Zhao, Y.; Kim, Y.−H.;A. Dillon, M. Heben, Zhang, S., *Phys. Rev. Lett.*, **94**, 1555041 (2005).
46. S. Asuha, H.Y. Zhao, Wu, L. Song, O. Tegus, *J. Alloys Compounds*, **472**, 23 (2009).
47. G. Zu, J. Shen, X. Wei, X. Ni, Z.Zhang, J. Wang, G. Liu, *J. Non-Cryst.Solids*, **357,** 2903 (2011).
48. Y.S.C. Lee, *J. Mater. Sci*., **27**, 5203 (1992).
49. F. Cao, L. Ren, X. Li, *RSC Adv.*, **5**, 18025 (2015).
50. V.A. Radzig, A.A. Ischenko, *Kinetics&Catalysis*, **52**, 316 (2011).
51. Y. R. Katsobashvili, N. S. Kurkova, M. M. Getsiu, Bull. Acad. Sci. USSR, Division Chem. Sci. **19**, 1003 (1970).
52. A.R. Stokes, *Proc. Phys. Soc. (London), A*, **61**, 382 (1948).
53. J.L. Bahr E.T. Mickelson, M.J. Bronikowski, R.E. Smalley, J.M. Tour, *Chem. Commun.*, **2**, 193 *(*2001).
54. J.L. Hudson, M.J. Casavant, J.M. Tour, *J. Am. Chem. Soc.*, **126**, 11158 (2004).
55. V.A. Sinani, M.K. Gheith, A.A. Yaroslavov, A.A. Rakhnyanskaya, K. Sun, A.A. Mamedov, J.P. Wicksted, N.A. Kotov, *J. Am. Chem. Soc.*, **127**, 3463 (2005).
56. A.P. Hynes, R.H. Doremus, *J. Am. Ceram. Soc.*, **74**, 2469 (1991).
57. S. H. Hong, G.L. Messing, *J. Am. Ceram. Soc* **81**, 1269 (1998).
58. F. I. Hurwitz, H. Guo, R.B. Rogers, E.J. Sheets, D.R. Miller, K.N. Newlin, M.K. Shave, A.R. Palczer, M.T. Cox, *J. Sol Gel Sci.Technol*., **64**, 367 (2012).
59. J.F. Poco, J.H .Satcher Jr., L.W. Hrubesh, *J. Non-Cryst. Solids*, **285,** 57 **(**2001).
60. A. Sedaghat, E.Taheri, *J.Adv.Mater.Process*, **2**, 25 (2014).
61. F. Haoa, J. Zhonga, P.-Le Liua,∗, K.i-Yi Youa, Ch. Weib, H.-Jie Liuc, He-An Luoa, *Chem*,. **351**, 210 (2011).